ELSEVIER

Polymer 40 (1999) 4673–4684

polymer

Modeling of helix reversal defects in polytetrafluoroethylene II. Molecular dynamics simulations[1]

D.B. Holt[a], B.L. Farmer[b,*]

[a]*Naval Research Laboratory, Center for Bio/Molecular Science and Engineering (6900), 4555 Overlook Ave., S.W., Washington, DC 20375, USA*
[b]*Air Force Research Laboratory, AFRL/MLBP, 2941 P Street, Suite 1, Wright–Patterson AFB, OH 45433-7750, USA*

Dedicated to Professor Ronald K. Eby on the occasion of his 70th birthday

Received 31 December 1998; accepted 19 January 1999

Abstract

Molecular mechanics and dynamics simulations have been utilized to probe the nature of helix reversal activity in polytetrafluoroethylene (PTFE). The results of the simulations indicated that helix reversals do form and migrate in PTFE crystals. At low and intermediate temperatures, the most important defect structure was a helix reversal band: two helix reversals which bracket a small chain segment having the opposite helical sense from the parent molecule. The size of this reversal band defect was equal to approximately half of the helical repeat unit in the low and intermediate temperature phases. In the high temperature phase where intermolecular effects are diminished, a wider distribution of reversal band sizes was observed during the simulations. The impact of helix reversal activity on rotational disorder was also examined. In addition to the rotational disorder created by the presence and motion of helix reversals, a mechanism was identified by which significant reorientation of a chain segment (having the same helical sense as the host chain) about the molecular axis can occur when it is bracketed by two helix reversal bands.

Keywords: Polytetrafluoroethylene; Helix reversal defects; Molecular dynamics

1. Introduction

The helical structure of polytetrafluoroethylene (PTFE) gives rise to a very rich phase behavior for this chemically simple polymer. At atmospheric pressure and within a few tens of degrees Celsius, PTFE exhibits three solid state phases. In phase II below 19°C, X-ray and electron diffraction data indicate that the material has a well ordered triclinic unit cell containing two chain stems of opposite hand [1]. The molecules have a 54/25 (u/t, units per turn) helical conformation, though a 13/6 ratio is more often quoted. At 19°C, an order–disorder transition occurs [2]. The disorder which comes into play is reorientation (rotations) of the molecules about their axes (not reorientation of helical axes). The molecules also untwist slightly to adopt a 15/7 conformation. This intermediate phase (IV) has a metrically hexagonal unit cell containing one stem (based on X-ray data) and persists up to 30°C. Model calculations have also shown that larger cells (also consistent with diffraction data) containing both left- and right-handed helices are feasible [3]. Above 30°C, further rotational disordering and untwisting of the helices occurs as temperature increases. In this high temperature phase I, the 15/7 helical conformation gradually gives way to a time-averaged 2/1 (planar zigzag) conformation as the temperature increases [3]. The unit cell remains metrically hexagonal.

Though X-ray data suggest a high degree of order when PTFE is at or below 19°C, other experimental techniques such as solid state nuclear magnetic resonance (NMR) and Raman scattering suggest that dynamic disorder exists in crystalline regions even at cryogenic temperatures [4,5]. To reconcile these conflicting observations, the presence and mobility of chain defects called helix reversals were postulated [4]. Such helix reversals could allow large rotations about molecular axes locally without affecting the long-range order observed in X-ray diffraction studies. It was further suggested [4] that helix reversals on neighboring chains could interact and segregate onto well defined planes within a PTFE crystal, and that these planes of defects could travel through the crystal.

The phase and mechanical behavior of fluoropolymers depend on chain and segmental motions. Thus, they are

* Corresponding author. Tel.: +1-937-255-9209; fax: +1-937-255-9157.

E-mail address: farmerbl@ml.wpafb.af.mil (B.L. Farmer)

[1] Work was carried out the the University of Virginia, Charlottesville, VA 22903-2442, USA.

0032-3861/99/$ - see front matter
PII: S0032-3861(99)00076-2

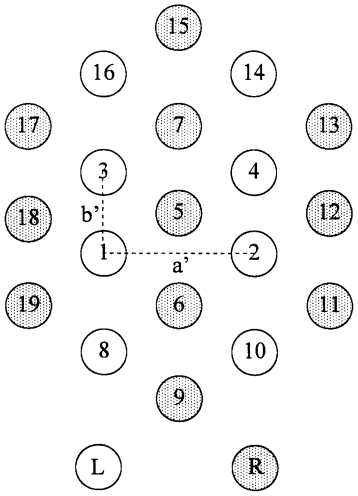

Fig. 1. Schematic diagram of the nineteen chain cluster and important crystallographic directions.

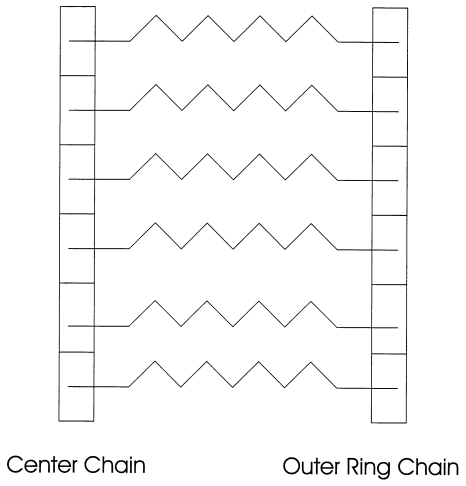

Fig. 2. Schematic of substructuring and distance restraints placed between center chain and outer ring chains.

subject to the influences of helix reversal activity. Though understood conceptually, details of the relationships between helix reversals, rotational disorder, phase transitions, and mechanical properties in fluoropolymers are still unclear. This article describes the results of molecular dynamics simulations which allow direct observation of molecular events and elucidate the nature of intra- and intermolecular interactions between helix reversals and chain rotations.

2. Methods

2.1. Molecular dynamics simulations

Molecular dynamics simulations on a cluster of nineteen F–$(CF_2)_{60}$–F chains (Fig. 1) were used to investigate the disordering chain motions that occur in fluoropolymers. The simulations were performed for temperatures of 100, 200, 248, 273 and 298 K. As the order–disorder phase transition in perfluoroeicosane ($C_{20}F_{42}$) occurs at 200 K [6], it was suspected that the behavior of the model would more closely mirror that found in crystals of perfluorocarbon oligomers than PTFE, with disorder and transitions occurring at lower temperatures due to the lack of rotational constraints. In addition, it has been shown in previous modeling studies that decreased lamellar thickness leads to lower transition temperatures in PTFE [2].

Table 1 gives the molecular dynamics control parameters used in all of the simulations. For the heating stages, initial velocities were assigned based upon a Boltzmann distribution at 50 K. The temperature was increased by 50 K every 50 fs up to 100 K, or 200 K. For the 248 K simulation, the cluster was heated to 200 K as described earlier, and then a 48 K increment was made to reach the target temperature. For the 273 and 298 K simulations, the 50 K/50 fs protocol was used up to 250 K before making the 23 and 48 K increments, respectively, to reach these target temperatures.

Distance restraints on the outer chains were used to prevent the cluster from disassembling. A substructuring scheme of six segments each containing 10 CF_2 groups was used (see Fig. 2). Energy versus displacement curves for the a' and b' directions (Fig. 1) were generated for the center chain (Chain 5) in the cluster by stepping it in those directions in 0.25 Å increments and calculating the energy difference relative to a freely minimized cluster. All chains were held conformationally rigid during these calculations. A quartic function, shown in Eq. (1), was required to adequately fit the energy versus displacement profiles.

$$E = k_4 d^4 + k_3 d^3 + k_2 d^2 + k_1 d \quad (1)$$

where k_i are the force constants and d is the displacement from the equilibrium position. The constants that resulted

Table 1
Molecular dynamics control parameters

Simulation time	200 ps (300 ps for 100 K simulation)
Temperature control	Andersen method
Non-bond cutoff	9.5 Å
Integrator	Velocity Verlet
Time step	2 fs
Snapshot interval	500 fs

Table 2
Constants for quartic distance restraints (Eq. (1)). Units are kcal/mol

	a'-direction[a]	b'-direction
k_4	251.57	213.33
k_3	37.24	− 11.25
k_2	60.68	84.39
k_1	3.07	0.81

[a] See Fig. 1.

from this process are shown in Table 2. These were then used to restrain the outer chains of the model.

The force field used to describe intra- and intermolecular interactions of perfluorocarbon molecules is given in the first paper in this series. This set of parameters is far superior to a force field that was previously derived and used in some earlier simulations [7]. The current force field was established using a much larger range of helical conformations than was used for generating the earlier parameter set. More importantly, the van der Waals parameters utilized in the current work yield intermolecular distances which are closer to experimental values than do those from the previous force field.

Torsional restraints were placed on the dihedrals at the ends of the chains to lessen the probability of the chain termini becoming initiation sites for helix reversals. This increases the effective chain length. To increase the resistance to torsional motion of the chain ends, scaling factors were applied to the energy and derivatives for the dihedrals formed by C1–C2–C3–C4 (τ1), C2–C3–C4–C5 (τ2), C56–C57–C58–C59 (τ56), and C57–C58–C59–C60 (τ57) on each chain. Values of the scaling factors were derived in the following manner. The most mobile helix reversal defect structure involves a minimum of two dihedrals. Setting two consecutive dihedrals in the center of Chain 5 (see Fig. 1) to *trans* (180°) resulted in an energy increase of 22.9 kcal/mol for the nineteen chain cluster (referenced to the energy of the fully minimized cluster).

Setting the two end torsions to *trans* increased the energy of the cluster by 2.16 kcal/mol. It was assumed that contributions from the individual dihedrals to the total energy barrier are additive. Therefore, in the interior of a crystal, where all torsions have essentially the same environment, an individual dihedral would see a barrier of 11.45 kcal/mol (0.5 × 22.9 kcal/mol). Setting τ1 and τ2 individually to *trans* increased the cluster energy by 0.63 kcal/mol and 1.46 kcal/mol, respectively. The sum of these individual contributions (2.09 kcal/mol) is not too different from the energy increase (2.16 kcal/mol) observed when both end torsions were set to *trans* simultaneously. The scaling factors were taken to be the ratios of the assumed individual barrier (11.45 kcal/mol) for a torsion in the interior of a crystal to those seen by the dihedrals at the chain termini. For τ1 and τ57, the scale factor was 11.45/0.63 = 18.17, while for τ2 and τ56, it was 11.45/1.46 = 7.84.

2.2. Simulated X-ray diffraction patterns

The calculation of diffraction patterns from the cluster is a convenient method for summarizing structural characteristics. It also provides a link between the model/simulation data and experimental data. The Diffraction module available in the CERIUS^2 (version 3.0) molecular modeling package was used to calculate time-averaged fiber diffraction patterns from the cluster as it evolved during the last 25 ps of the molecular dynamics simulations. The fiber pattern from a static, minimized nineteen chain cluster is shown in Part 1 of this series. The coordinates of the structure were considered at 2.5 ps intervals for the diffraction pattern calculations. Therefore within the 25 ps period, ten ''snapshots'' of the cluster were averaged. The X-ray wavelength considered was 1.54178 Å, corresponding to Cu Kα radiation. Reciprocal space coordinates (Q) were scanned in 0.1 Å^{-1} increments (2θ increments of 1.580°) between Q = 0.0 and 6.0. Therefore, the 6.0 Å^{-1} by 6.0 Å^{-1} ''film'' was sampled at 3600 points. Q, the magnitude of the scattering vector, is defined as

$$Q = (4\pi\sin\theta)/\lambda. \quad (2)$$

Cylindrical averaging was applied to the scattering along with a model size correction to reduce the size of the peak at the origin of reciprocal space. The correction subtracts the cylindrically averaged scattering from a cylinder of uniform scattering density [8]. The length and radius of the correction cylinder were optimized by the CERIUS^2 software based on the dimensions of the nineteen chain cluster.

3. Results

Before proceeding with a description of the results, it must be stated that no data from the simulation at 298 K will be presented or discussed. The results were essentially identical to those from the 273 K simulation.

3.1. Helix reversal activity

For each of the dynamics simulations, the activity of helix reversals was monitored as follows. The helical sense of the chains was plotted as a function of time and position by applying a grayscale coding such that left-handed torsions were assigned white, right-handed torsions black, and near *trans* dihedrals with values between ± 5° (*trans* = 0.0° in this case) were coded gray. As the development of disorder as well as equilibrium behavior is of interest, helix reversal activity plots were generated for the entire duration of each simulation. These are shown in Fig. 3(a)–(d).

Fig. 3(a) depicts the helix reversal activity on Chains 1–5 (see Fig. 1) during the 100 K simulation. The many grey ''dots'' indicate transient, near-*trans* dihedrals. Most of these near-*trans* torsions occur singly or in pairs. Inspection of the dihedral trajectories revealed that essentially all of the near-*trans* torsions were of the same hand as the parent chain, even those involved in a near-*trans* pair. Accordingly, the helix reversal density given in Table 3 for the 100 K simulation is close to zero. Note that near-*trans* dihedrals were not excluded from this count. The kinetic energy of the torsional motion was not sufficiently high at this simulated temperature to surmount the barrier to helix reversal formation.

The striking characteristic during the 200 K simulation is the development of well-defined bands that have the opposite helical sense from the host chains (Fig. 3(b)).

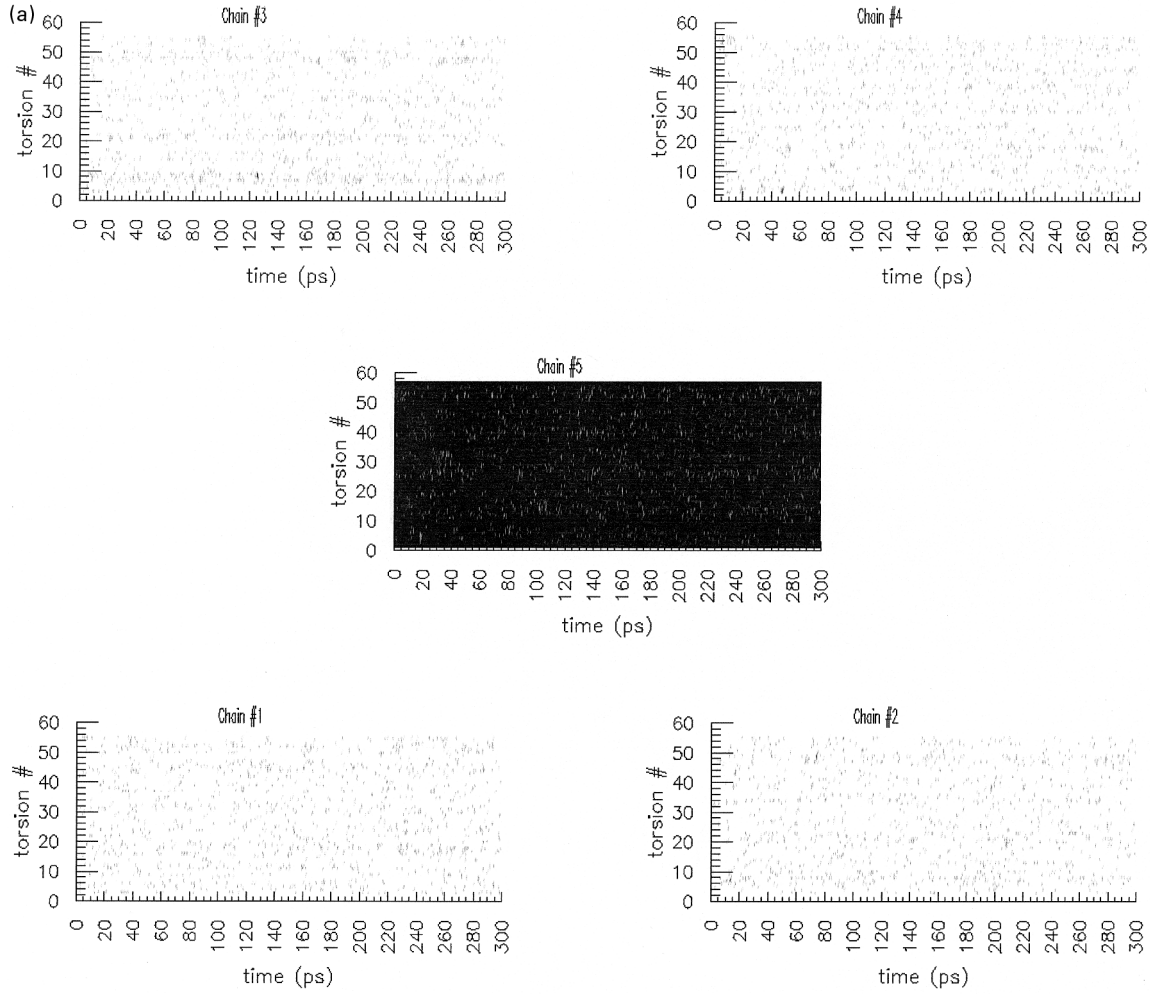

Fig. 3. Helix reversal activity during the (a) 100 K simulation, (b) 200 K simulation, (c) 248 K simulation, (d) 273 K simulation.

Structurally, the bands consist of a pair of helix reversals separated by a short chain segment that is of opposite helical sense relative to the parent chain. The formation and growth of a helix reversal band involve the appearance of an adjacent pair of helix reversals at some location within a chain, and subsequent migration of the individual helix reversals in opposite directions. These bands vary in thickness, but typically involve two to five dihedrals (five to eight backbone C atoms) and are flanked by near-*trans* torsions. The near-*trans* dihedrals are necessary to maintain the linearity of the helical axes and minimize lattice strains. There is no preferred direction of motion for these reversal bands. They undergo small fluctuations and maintain relatively stable positions in the cluster. Larger excursions with velocities near 100 m/s also occurred. See Chain 1 in the vicinity of Torsion #40 between 140 and 160 ps (the axial distance between two adjacent dihedrals is ~ 1.3 Å).

The helix reversal bands on neighboring chains of the same hand (1, 2, 3 and 4) prefer to be staggered axially; i.e. they do not tend to arrange themselves into planes normal to the chain axes. Intermolecular interactions of reversal bands on chains of opposite helical sense are difficult to discern from Fig. 3(b). Inspection of plots (not shown) of helix reversal behavior on other chains in the cluster did not suggest strong, persistent intermolecular coordination of helix reversal behavior on chains of opposite hand.

The plots of helix reversal behavior for the 248 K simulation (Fig. 3(c)) indicate that the reversal bands have a higher mobility at this temperature than at 200 K and are present in much greater numbers (see Table 3). Excursion velocities near 160 m/s are observed. Thicker reversal bands involving up to 10–12 dihedrals (13–15 backbone C atoms) are also present, but do not appear to be as mobile as the smaller defects. With the greater motion and numbers of the reversal defects, the axial staggering of reversal bands on neighboring like-handed chains observed at 200 K is not as readily apparent at 248 K.

The helix reversal behavior at 273 K is shown in Fig. 3(d). Compared to that during the 248 K simulation, there is an insignificant increase in the density of helix reversals (see Table 3) and in the thickness of the reversal bands.

Higher excursion velocities near 250 m/s were observed. The density of helix reversal defects increased with

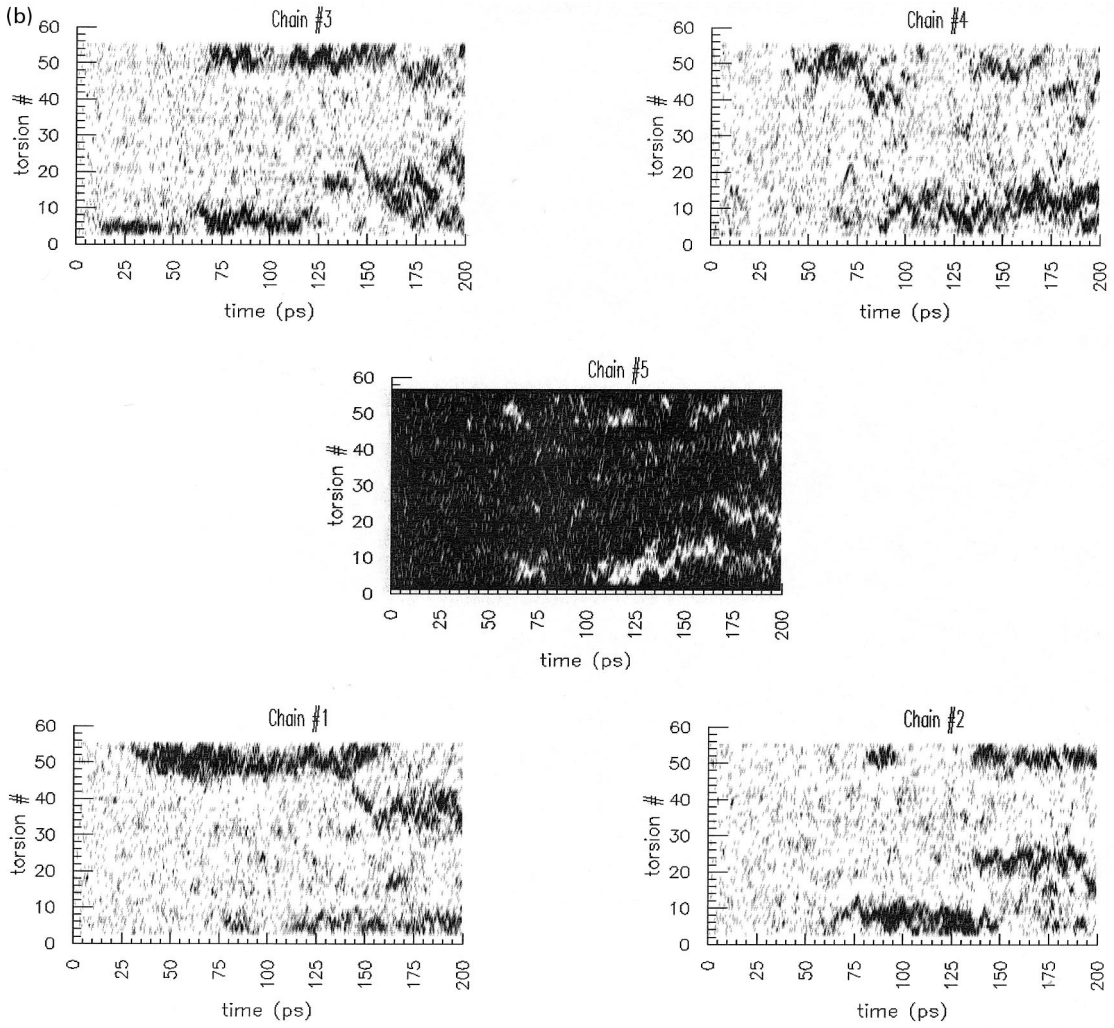

Fig. 3. (*continued*)

temperature in the simulations. Significance testing (with the *t*-test) indicated that the helix reversal density increases between the 100, 200 and 248 K simulations were statistically significant (at 99% confidence or better). Therefore the increase on average of nine and five reversals, respectively, at successively higher temperatures was significant.

The plots of helix reversal activity indicate the range of values into which the backbone dihedrals fall, but do not reveal the magnitude of torsional motions which are responsible for helix reversal formation. These data are presented in Table 4. At 100 K, the torsional amplitude is not large enough to cause a reversal of hand. At 200 K, the average dihedral fluctuation amplitude is not large enough for the creation of helix reversals, but the larger oscillations contributing to the average allow the formation of a few reversals. At 248 K, the torsional amplitude is sufficient to allow helix reversals to form readily.

3.2. Rotations/librations about the chain axes

Rotations about the helical axes were examined by calculating an average setting angle trajectory for the central twenty CF_2 groups in each chain referenced to a defect free helix of appropriate hand and with a setting angle of zero degrees. Individual chain rotation trajectories are presented as needed to highlight specific behavior(s) under discussion. As it is often difficult to see correlations in ''raw'' dynamics trajectories which fluctuate rapidly, correlation coefficients over the last 50 ps of each simulation were calculated between the rotational trajectories of the chains with the following equation:

$$c_{AB} = \frac{N\Sigma A_n B_n - \Sigma A_n \Sigma B_n}{[(N\Sigma A_n^2 - (\Sigma A_n)^2)(N\Sigma B_n^2 - (\Sigma B_n)^2]^{1/2}}. \quad (3)$$

In this particular case, A_n and B_n are values of setting angles of the central segments of two different chains, A and B, at time step n. These data are shown in Table 5.

The actual values of c_{AB} in the table and averages of the absolute values, $|c_{AB}|$, of the correlation coefficients are not the most important pieces of information in these data. They all indicate very weak coordination of rotational and

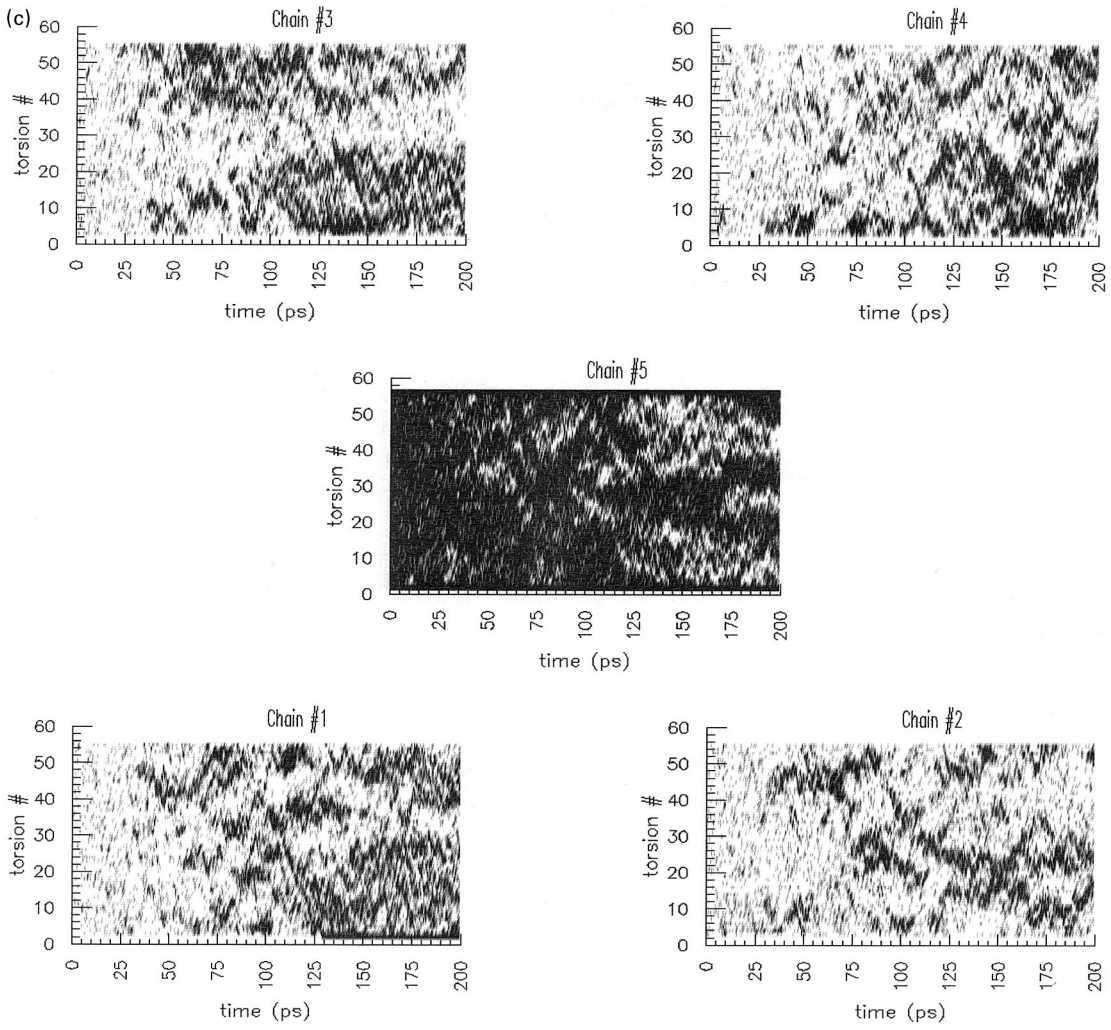

Fig. 3. (*continued*)

librational motion, and the mean absolute values of the correlation coefficients at each temperature are not statistically different from each other. However, the sign (positive or negative) of the correlation coefficient for a given pair of chains is very noteworthy. The sign is indicative of the relative directions of rotations/librations of two chains. A positive value indicates rotation in the same direction, while a negative value signifies rotation in opposite directions. For the 100 and 200 K simulations, a well-defined pattern is maintained. Like handed chains tended to rotate/librate in the same direction, and the motions of chains of opposite helical sense tended to be in opposite directions. These relationships did not hold very strongly during the 248 and 273 K simulations in which the chiral identity of the chains was lost.

The amplitudes of setting angle fluctuations are given in Table 6. As expected, these amplitudes increase with temperature. Note that the libration amplitude for the low temperature simulation (100 K) is close to 6.7°. This is the ''notch'' angle (360°/54 = 6.7°) for PTFE chains in the low temperature phase II in which the helical conformation determined from X-ray diffraction data is 54/25 [1]. Further simulations would be required to determine if the approximate doubling of the libration amplitude at 200 and 248 K is significant. The substantial increase in the average libration amplitude (and standard deviation) at 273 K was due to the onset of large, abrupt changes in setting angles.

3.3. Diffraction patterns

Calculated fiber diffraction patterns (averaged over the last 25 ps) for the 100, 200, 248 and 273 K simulations are shown in Fig. 4(a)–(d), respectively. The same contour levels were used in each plot. They show that three distinct phases were ultimately attained during the simulations. The helical conformation was 13/6 (2.167) at 100 K. (Note that the resolution of the calculated diffraction patterns is not sufficient to distinguish between 13/6 and 54/25 helices.) The conformation changed to 17/8 (2.125) at 200 K, and then to 2/1 at 248 K. It remained 2/1 during the 273 K simulation. This does not imply that these temperatures are the transition temperatures. The calculated diffraction

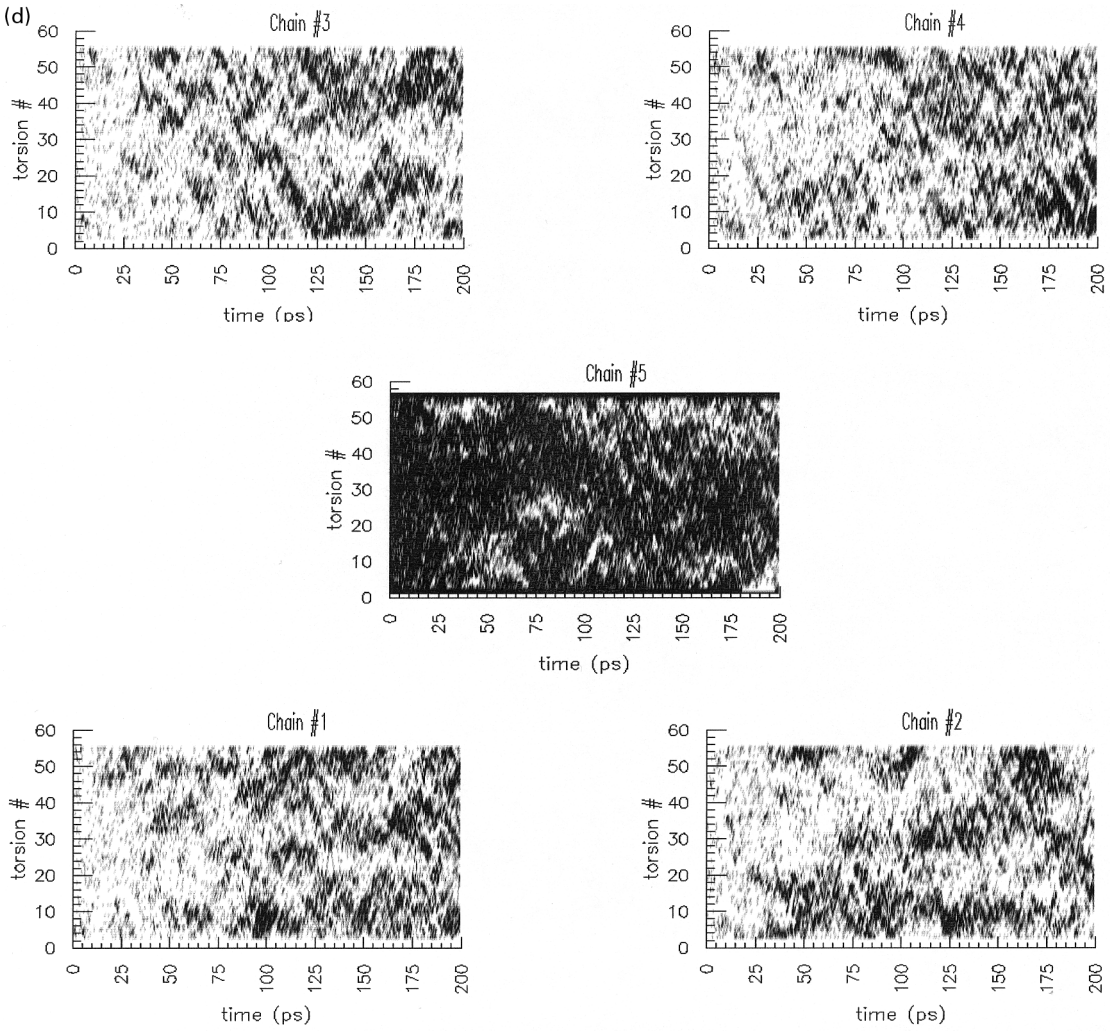

Fig. 3. (*continued*)

pattern of a static, freely minimized nineteen chain cluster (shown in Part I) indicated that the helical conformation was 13/6. Note that the intensity of the reflections on the second layer line, which are highly sensitive to rotational disorder, have fallen below the threshold for the minimum contour value plotted in the 200 K and higher temperature simulations. These diffraction patterns are very similar to those observed experimentally in PTFE, in which the helical conformation progresses from 54/25 (2.160) in Phase II to 15/7 (2.143) in Phases IV and I, and eventually to 2/1 at high temperatures [1,3].

Table 3
Average helix reversal densities during the simulations. Values are the population averages for Chains 1–5 over the last 50 ps of each simulation. Near-*trans* torsions are not excluded from these counts

Temperature (K)	Number per chain
100	0.2 ± 0.6
200	9.3 ± 2.5
248	14.2 ± 3.2
273	14.3 ± 3.1

The cluster of PTFE chains also experienced thermal expansion during the simulations. Table 7 gives *d*-spacings for the equatorial reflections from the calculated fiber patterns in Fig. 4(a)–(d). A Gaussian curve was fit to the data to determine the location of the peak. The *d*-spacings in Table 7 are in reasonable agreement with experimental values, 4.866 and 4.902 Å, for PTFE in Phases II and IV, respectively [9]. The similarity of the simulated structures to those observed experimentally demonstrates the quality of the force field.

3.4. Thermodynamic properties

It is possible to derive a variety of useful properties of model systems such as heat capacities or coefficients of thermal expansion (CTEs) by applying statistical mechanical relations to fluctuations of quantities such as energy or volume which occur during a molecular dynamics

Table 4
Mean dihedral angle fluctuations. Values are the population averages of time-averaged backbone dihedral fluctuations occurring in Chains 1–5 over the last 50 ps of each simulation

Temperature (K)	Avg. $\langle\Delta\tau\rangle$
100	4.5 ± 0.5°
200	10.4 ± 2.5°
248	12.9 ± 2.0°
273	13.6 ± 1.5°

simulation [10,11]. In addition, properties which are derivatives of a state variable with respect to temperature may be determined from a single simulation at a single temperature. This method is generally more accurate than taking the difference of average properties for two simulations at different temperatures, and then dividing by the temperature difference [12].

Fluctuations in total energy (the Hamiltonian) may be used to obtain constant volume heat capacities at the four simulated temperatures, which may then be compared with experimental values. The appropriate statistical mechanical relation for the canonical ensemble is

$$\langle\delta E^2\rangle_{\mathrm{NVT}} = \mathrm{k_B} T^2 C_{\mathrm{v}} \tag{4}$$

where $\langle\delta E^2\rangle_{\mathrm{NVT}}$ is the variance of the fluctuations in total energy of the system and $\mathrm{k_B}$ is the Boltzmann constant. To evaluate C_{v} from the molecular dynamics data, the energy fluctuations were averaged over the last 50 ps of the simulations. Values of C_{v} derived using Eq. (4) are given in Table 8. They are in fair agreement [9] with heat capacities (constant pressure) determined experimentally for PTFE which range from 19.4 J/mol CF_2/K at 100 K to 45.1 J/mol CF_2/K at 298 K. The increased value of C_{v} derived from the 100 K simulation indicates that this temperature was likely near a transition temperature for the model system in this study. Similar behavior is observed in heat capacities derived from differential scanning calorimetry measurements on perfluoro-*n*-alkanes [13]. Peaks in heat capacity–temperature data occur for these materials just before disordering transitions in the solid state. Small amplitude conformational and rotational disorder were observed during the 100 K simulation. Therefore, an assignment of the disorder (conformational, rotational, or both) responsible for the increase in heat capacity at 100 K cannot be made without data from at least one additional simulation at a temperature below 100 K. Nevertheless, this agreement of C_{v} values derived from the simulations with experimental values is another demonstration of the quality of the force field.

Table 5
Correlation coefficients c_{AB} over the last 50 ps for rotational/librational motion about the molecular axes. Values of the A and B indices correspond to the chain numbers indicated for each column and each row

(a) 100 K simulation

Chain	1	2	3	4	5
1	1.0	0.38	0.38	0.19	− 0.31
2		1.0	0.22	0.18	− 0.23
3			1.0	0.24	− 0.47
4				1.0	− 0.09
5					1.0

Average for all chains: $|c_{\mathrm{AB}}| = 0.26 \pm 0.11$

(b) 200 K simulation

Chain	1	2	3	4	5
1	1.0	0.38	0.63	0.34	− 0.36
2		1.0	0.30	0.33	− 0.20
3			1.0	0.18	− 0.30
4				1.0	− 0.29
5					1.0

Average for all chains: $|c_{\mathrm{AB}}| = 0.33 \pm 0.12$

(c) 248 K simulation

Chain	1	2	3	4	5
1	1.0	0.15	0.29	− 0.28	0.17
2		1.0	− 0.01	− 0.06	0.14
3			1.0	− 0.29	0.16
4				1.0	− 0.28
5					1.0

Average for all chains: $|c_{\mathrm{AB}}| = 0.18 \pm 0.10$

(d) 273 K simulation.

Chain	1	2	3	4	5
1	1.0	− 0.01	− 0.31	− 0.12	− 0.17
2		1.0	0.37	0.29	0.12
3			1.0	0.28	0.58
4				1.0	0.08
5					1.0

Average for all chains: $|c_{\mathrm{AB}}| = 0.23 \pm 0.17$

4. Discussion

The results of the molecular dynamics simulations confirm that the helix reversals play an important role in the behavior and properties of PTFE. However, at low and intermediate temperatures, the distribution of helix reversals is not uniform. Rather, the helix reversals are more closely spaced than a uniform distribution would indicate as a result of the mechanism required for formation. An isolated helix reversal cannot form spontaneously in the middle of a chain (as this would require a large number of torsions to change hand simultaneously) but may form at a chain terminus and migrate. However, a reversal pair can form in the middle of a chain via coordinated torsional motion of two dihedrals. The pair may then drift apart. This results in a small segment of chain with helical sense opposite to that of the host molecule and which can behave as a single entity. This defect can involve as few as two dihedrals (five $-CF_2-$ groups), or be comprised of larger segments with lengths approaching *c*-axis repeat distances (13–15 $-CF_2-$ groups). This result is in accordance with earlier suggestions that chain segments containing between five and thirteen $-CF_2-$ groups are responsible for relaxations in PTFE and TFE-HFP copolymers [14]. The larger size defect structure has been discussed previously and referred to as a coherent twin

Table 6
Average rotational/librational fluctuations during the simulations during the last 50 ps of the simulations

Temperature (K)	$\langle\phi_{rms}\rangle$
100	5.9 ± 0.6°
200	13.5 ± 1.5°
248	15.7 ± 4.2°
273	24.6 ± 12.3°

Table 7
Equatorial *d*-spacing derived from the calculated diffractions patterns in Fig. 4(a)–(d)

Temperature (K)	*d*-spacing (Å)
100	4.983
200	5.018
248	5.030
273	5.032

helix reversal defect if its length (and number of $-CF_2-$ groups) is equal to the helical repeat distance [15]. It was further proposed that the coherent twin defect would be the dominant defect structure found in the intermediate phase (IV) of PTFE.

The results of the intermediate temperature simulation (200 K) in this study suggest that the smaller size reversal band may dominate behavior in the intermediate temperature phase. The helix reversal band structures at 200 K (Fig. 3(b)) indicate that coherent (as defined earlier) twin helix reversal defects, which would consist of 17 $-CF_2-$ groups (14 dihedrals) for the model at 200 K, were not the predominant defect structures. Rather, the reversal bands were approximately half this size on average (5–6 dihedrals including near-*trans* torsions). This suggests that the reversal band size may still be related to the helical conformation in a given phase. However, as only one intermediate temperature was simulated, it is possible that the small structures are involved in the behavior in the lower temperature range of the intermediate phase, and that the size of the predominate defect increases with temperature into the upper range of the intermediate phase.

It is quite possible that free chain termini could serve as ''nucleation'' sites for larger reversal defects in the intermediate phase. Fig. 3(b) provides evidence for this. Thicker reversal bands persist on Chains 1 and 2 at or near the chain ends. During the simulations at the higher temperatures, in which the distribution of helix reversals became more uniform, larger reversal bands occurred more frequently (Fig. 3(c) and (d)). This indicates that in a PTFE crystal at

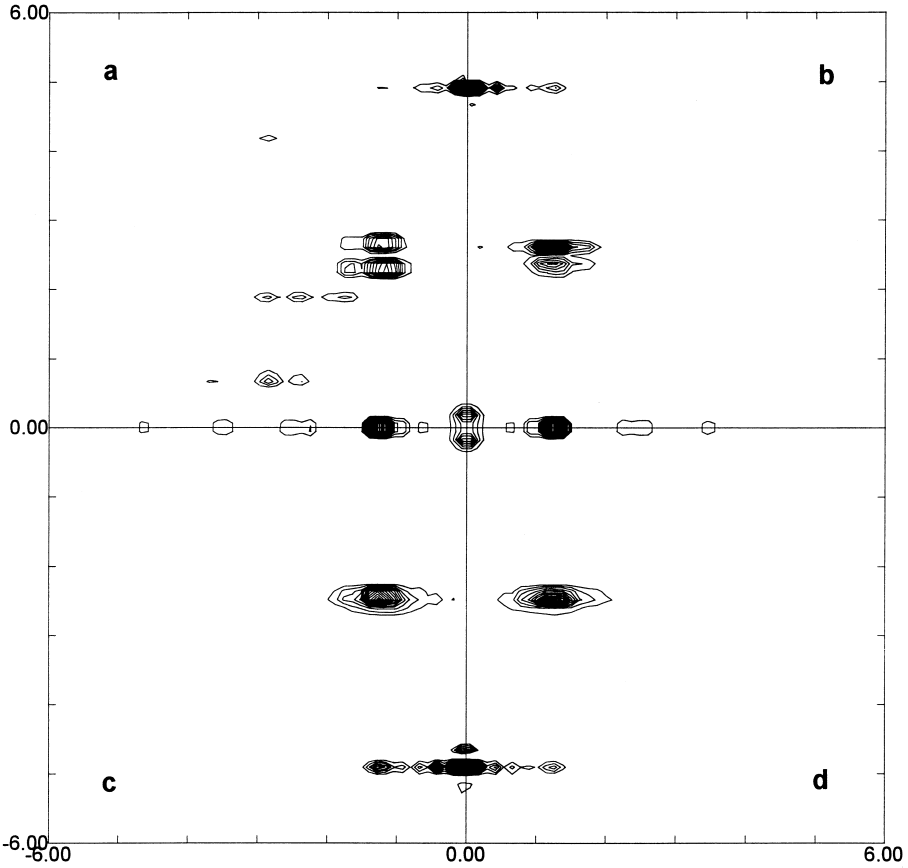

Fig. 4. Quadrants of the calculated fiber diffraction patterns over the last 25 ps of the simulations. (a) 100 K, (b) 200 K, (c) 248 K, (d) 273 K.

Table 8
Heat capacities derived from energy fluctuations during the simulations

Temperature (K)	C_v (J/mol CF_2/K)
100	36.6
200	22.4
248	30.8
273	32.1

low and intermediate temperatures, the activation barrier for creating a reversal band defect is a function of the length of the defect. At high temperatures where intermolecular effects are diminished, this length dependence is weakened. For an isolated molecule, for which there are no intermolecular interactions, molecular mechanics calculations (Part I) showed that the energy cost of creating helix reversal band defects was essentially constant after three or more dihedrals were involved.

Small helix reversal bands were more mobile than larger defect segments. The highest velocities of reversal bands encountered in the nineteen chain cluster during the simulations, 100–250 m/s, are in agreement with previous estimates of velocities of singular reversals near chain ends [16]. These are much lower than the velocity of a transverse (shear) sound wave in bulk PTFE [9] which propagates around 770 m/s. This is another check on the validity and accuracy of the results. The maximum velocity of defects in a crystal cannot be greater than the speed of sound in the crystal.

The simulation results indicate that a fundamental change in intermolecular relationships occurs between the phases exhibited by fluoropolymers along with the changes in helical conformation. The amplitude of librations followed the expected trend of increasing with temperature as shown in Table 6, but the relative directions of librations and rotations of the central segments of neighboring chains exhibited two different relationships as suggested by the correlation coefficients in Table 5 (a)–(d). During the low and intermediate temperature simulations (100 and 200 K), chains of the same hand generally rotated/librated in the same direction, while pairs of chains with opposite helical sense did so in opposite directions. This behavior is consistent with results from previous modeling studies which indicated that helices of opposite sense would likely rotate in opposite directions [17]. During the 248 and 273 K simulations, this pattern did not hold. Pairs of initially like-handed chains had opposite rotational relationships, and pairs of initially opposite-handed molecules no longer consistently maintained the opposite rotation/libration directionality observed in the low temperature simulations. The helix reversal activity plots (Fig. 3(a)–(d)) show that the cause of this change in rotational/librational behavior is a loss of identity in handedness (relative to initial helical sense) of the chain segments as the density of conformational defects increases at higher temperatures. The arrangement of right and left-handed chain segments is far different from the initial arrangement of molecules, each of which was characterized by a single helical sense.

The role of helix reversal defects in the rotational disorder observed in fluoropolymers can be classified into two major influences: one static and one dynamic. (1) The mere presence of a helix reversal or reversal band causes a disruption of the local setting angle and results in rotational disorder. (2) If the defect migrates, the disruption of the local setting angle becomes dynamic and will fluctuate as helix reversal defects move along a given chain.

A third manner in which helix reversal defects may influence dynamic rotational disorder is suggested by the results of the simulations in this study. Comparison of the plots of helix reversal activity with the rotational trajectories reveals an interplay of helix reversal and chain segment reorientation behavior. During the 200 K simulation, Chains 1 and 3 show low frequency (compared to librations) changes in their setting angles between 150 and 175 ps. The rotational trajectory for Chain 1 is shown in Fig. 5. Chains 4 and 5 experienced similar changes in setting angle in this time interval. In accordance with rotational correlations described previously, these rotations were in the same direction for the like-handed chains (Chains 1,3,4), while the change in setting angle of Chain 5 occurred in the opposite direction. Examination of Fig. 3(b) between 150 and 175 ps reveals the presence of helix reversal bands bracketing the central sections of the molecules (over which the setting angle fluctuations were averaged) in this time interval. The plot for Chain 1 provides the best example. A short-lived reversal band at torsion #15 forms a bracket with a longer-lived band at torsion #38 between 160 and 170 ps.

This suggests a potential mechanism by which large rotations of chain segments about the molecular axes may occur. A pair of helix reversal bands or one reversal band and a free chain end bracketing a short chain segment (≤ 2 helical repeats) could effectively isolate that section of molecule from the rest and allow (or possibly cause) it to rotate more or less independently of the segments above and below it. This will be subsequently referred to as the IRS (Independently Rotatable Segment) mechanism. Instances in Fig. 3(b) in which persistent reversal bands bracket longer sections of the chains were not found to be associated with changes in the rotational/librational behavior of the segment.

Instances of the IRS mechanism were observed at all simulated temperatures (except 100 K). Another example can be seen by comparing the helix reversal behavior in Fig. 3(d) and the rotational trajectory of the central segment of Chain 3 during the 273 K simulation in Fig. 5. A large, abrupt change in setting angle, likely facilitated by a pair of helix reversal bands, occurs at 160 ps. However, a modification must be made to the IRS mechanism as it applies to the behavior observed during the higher temperature simulations (248 and 273 K). The increased helix reversal density and uniformity of distribution at higher

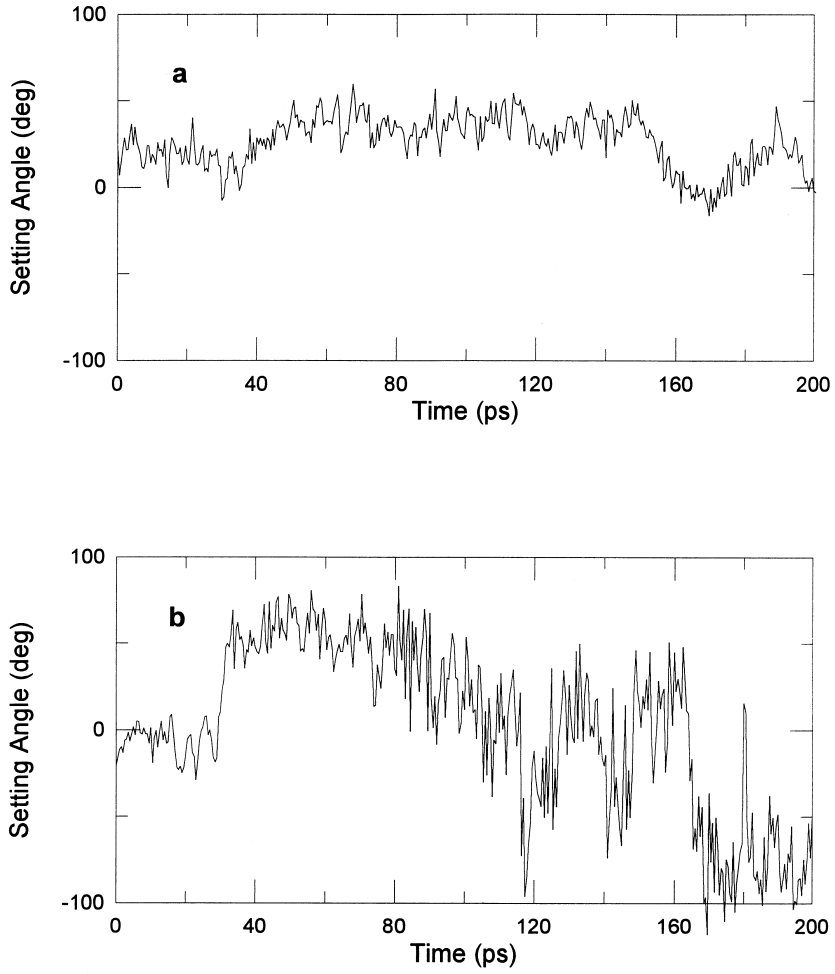

Fig. 5. Rotational/librational trajectory averaged over the central twenty CF_2 groups of (a) Chain 1 during the 200 K simulation, (b) Chain 3 during the 273 K simulation.

temperatures makes the assignment of a majority handedness to a given chain difficult. The concept of small bands of reversed hand in a chain of well defined helical sense gives way to one of alternating right- and left-handed segments (approximately of equal size), each of which is likely to be independently rotatable at higher temperatures. This version of IRS has been hinted at previously in the literature [15] (coherent twin reversal defect). Whether the rotation of a given segment is due to IRS or to the fact that it is part of a reversal band, the results of these simulations are in agreement with experimental studies from which it was estimated that the length of segment responsible for relaxation in fluoropolymers was between five and thirteen $-CF_2-$ groups [14].

5. Conclusion

Molecular dynamics simulations at several temperatures have shown that it is possible to predict the known temperature dependent behavior of fluoropolymers without restricting intra- or intermolecular degrees of freedom to conform to values characteristic of PTFE in a given phase. The results of the simulations strongly support the suggestion that helix reversals form and migrate in PTFE crystals, and play important roles in the behavior of fluoropolymers. The most important defect structure is a helix reversal band: two helix reversals which bracket a small chain segment having the opposite helical sense from the parent molecule. The size of this reversal band defect may be dependent upon the helical conformation (approximately half of the helical repeat unit) in the low and intermediate temperature phases. In the high temperature phase where intermolecular effects are diminished, a wider distribution of reversal band sizes was observed during the simulations. The IRS mechanism was found to contribute significantly to rotational disorder by allowing significant reorientation of a chain segment about the molecular axis when it is bracketed by two helix reversal bands.

Recent advances in experimental techniques such as atomic force microscopy (AFM) and X-ray diffraction will likely provide data for comparison with the molecular

modeling results of this work. X-ray diffraction studies with femtosecond (10^{-15}) resolution using bench-top (instead of synchrotron) radiation sources have been reported [18]. Such techniques hold great promise for studies of the kinetic aspects of disordering in PTFE and other materials.

Acknowledgements

The authors gratefully acknowledge E. I. DuPont de Nemours and Company and the donors of the Petroleum Research Fund administered by the American Chemical Society for partial financial support for this work.

References

[1] Weeks JJ, Clark ES, Eby RK. Polymer 1981;22:1480.
[2] Weeks JJ, Sanchez IC, Eby RK, Poser CI. Polymer 1980;21:325.
[3] Farmer BL, Eby RK. Polymer 1985;26:1944.
[4] Clark ES. J Macromol Sci-Phys 1967;B1(4):795.
[5] Brown RG. J Chem Phys 1964;40(10):2900.
[6] Schwickert H, Strobl G, Kimmig M. J Chem Phys 1991;95(4):2800.
[7] Holt DB, Farmer BL, Macturk KS, Eby RK. Polymer 1996;37:1847.
[8] CERIUS^2 3.0 Analytical instruments, 1997. San Diego, CA: Molecular Simulations Inc., 1997.
[9] Mark JE, editor. Physical properties of polymers handbook. New York: AIP Press, 1996.
[10] Allen MP, Tildesley DJ. Computer simulation of liquids. Oxford: Oxford University Press, 1987.
[11] Davidson N. Statistical mechanics. New York: McGraw-Hill, 1962.
[12] Klunzinger PE, Eby RK. Polymer 1997;38:4769.
[13] Jin Y, Boller A, Wunderlich B, Lebdev BV. Thermochimica Acta 1994;234:103.
[14] Eby RK, Wilson FC. J Appl Phys 1962;33(10):2951.
[15] Kimmig M, Strobl G, Stühn B. Macromolecules 1994;27:2481.
[16] Heinonen O, Taylor PL. Polymer 1989;30:585.
[17] Farmer BL, Eby RK. Polymer 1981;22:1487.
[18] Rischel C, Rousse A. Nature 1997;390:490.